AD-A059 701 HARVARD UNIV CAMBRIDGE MA DIV OF APPLIED SCIENCES F/G 20/12
STRUCTURE AND FLOW OF AMORPHOUS ALLOYS.(U)
AUG 78 F SPAEPEN N00014-77-C-0002
UNCLASSIFIED TR-5 NL

1 OF 1
AD A059701

END
DATE FILMED
12-78
DDC

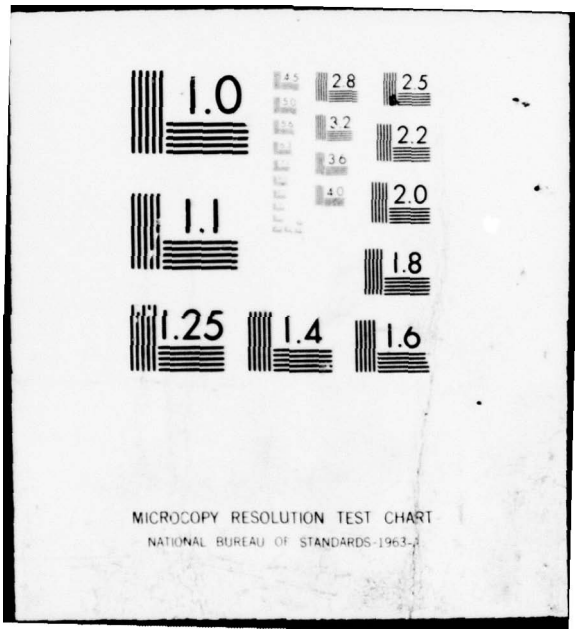
1.0
2.8
2.5
3.2
2.2
3.6
4.0
2.0
1.1
1.8
1.25
1.4
1.6
MICROCOPY RESOLUTION TEST CHART
NATIONAL BUREAU OF STANDARDS-1963-A

Office of Naval Research
Contract N00014-77-C-0002 NR-039-136

LEVEL

# STRUCTURE AND FLOW OF AMORPHOUS ALLOYS


By

Frans Spaepen



Technical Report No. 5



August 1978

Division of Applied Sciences
Harvard University • Cambridge, Massachusetts

Unclassified

SECURITY CLASSIFICATION OF THIS PAGE (When Data Entered)

| REPORT DOCUMENTATION PAGE | | READ INSTRUCTIONS BEFORE COMPLETING FORM |
|---|---|---|
| 1. REPORT NUMBER<br>Technical Report No. 5 | 2. GOVT ACCESSION NO. | 3. RECIPIENT'S CATALOG NUMBER |
| 4. TITLE (and Subtitle)<br>STRUCTURE AND FLOW OF AMORPHOUS ALLOYS | | 5. TYPE OF REPORT & PERIOD COVERED<br>Interim Report<br>6. PERFORMING ORG. REPORT NUMBER |
| 7. AUTHOR(s)<br>Frans Spaepen | | 8. CONTRACT OR GRANT NUMBER(s)<br>N00014-77-C-0002 |
| 9. PERFORMING ORGANIZATION NAME AND ADDRESS<br>Division of Applied Sciences<br>Harvard University<br>Cambridge, MA 02138 | | 10. PROGRAM ELEMENT, PROJECT, TASK AREA & WORK UNIT NUMBERS |
| 11. CONTROLLING OFFICE NAME AND ADDRESS | | 12. REPORT DATE<br>August 1978<br>13. NUMBER OF PAGES<br>41 |
| 14. MONITORING AGENCY NAME & ADDRESS(if different from Controlling Office) | | 15. SECURITY CLASS. (of this report)<br>Unclassified<br>15a. DECLASSIFICATION/DOWNGRADING SCHEDULE |

16. DISTRIBUTION STATEMENT (of this Report)

This document has been approved for public release and sale; its distribution is unlimited. Reproduction in whole or in part is permitted by the U. S. Government.

17. DISTRIBUTION STATEMENT (of the abstract entered in Block 20, if different from Report)

18. SUPPLEMENTARY NOTES

19. KEY WORDS (Continue on reverse side if necessary and identify by block number)

Review
Amorphous metals
Structural models
X-ray scattering
Chemical and topological short range order
Defects
Plastic flow

20. ABSTRACT (Continue on reverse side if necessary and identify by block number)

This paper, if it is to stay within reasonable limits, cannot possibly be as general as the title indicates. Therefore, rather than trying to cover all the recent developments in the study of structure and flow, an attempt will be made to provide a link between the two subjects: the emphasis will be on those structural aspects that are important for flow and on a description of the flow process that is as consistent as possible with the structural findings.

In a first section, recent developments in the study of the structure of amorphous alloys are reviewed. The discussion is limited to the transition

DD FORM 1 JAN 73 1473 EDITION OF 1 NOV 65 IS OBSOLETE
S/N 0102-014-6601

Unclassified
SECURITY CLASSIFICATION OF THIS PAGE (When Data Entered)

20. Abstract continued

metal-metalloid glasses, mainly because they are the oldest and best studied group. Significant progress has also been made in the study of metal-metal and rare earth-transition metal alloys, but these developments, although quite important, have not been included. It is shown how the new scattering techniques have confirmed earlier ideas about the high degree of short range order in the metal-metalloid glasses.

In amorphous systems as well as in crystals, atomic transport is governed by structural imperfections. As discussed in the second section, defects in amorphous metals are probably more diffuse than in crystals and can therefore best be described as individual sites with small perturbations of the local short range order.

In the third section this is applied to problems of steady state plastic flow. First, the experiments are reviewed by means of an empirical deformation mechanism map. Then, an attempt is made to describe the basic processes, homogeneous and inhomogeneous flow, from a unified point of view involving the concentration and motion of individual defect sites that produce local shear. Again, this implies a certain limitation in scope, since significant developments concerning transient flow, anelasticity, internal friction and embrittlement have not been included.

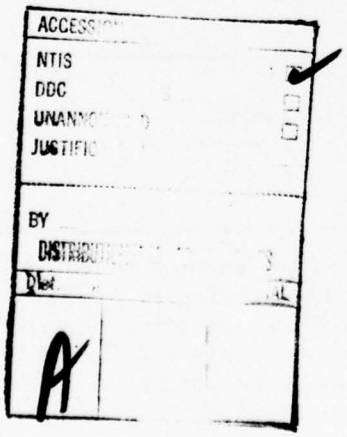

Office of Naval Research

Contract N00014-77-C-0002 NR-039-136

# STRUCTURE AND FLOW OF AMORPHOUS ALLOYS

By

Frans Spaepen

Technical Report No. 5

TR-5

August 1978

40 p.



The research reported in this document was made possible through support extended the Division of Applied Sciences, Harvard University, by the Office of Naval Research, under Contract N00014-77-C-0002.

Division of Applied Sciences

Harvard University · Cambridge, Massachusetts

# I. INTRODUCTION

This paper, if it is to stay within reasonable limits, cannot possibly be as general as the title indicates. Therefore, rather than trying to cover all the recent developments in the study of structure and flow, an attempt will be made to provide a link between the two subjects: the emphasis will be on those structural aspects that are important for flow and on a description of the flow process that is as consistent as possible with the structural findings.

In a first section, recent developments in the study of the structure of amorphous alloys are reviewed. The discussion is limited to the transition metal-metalloid glasses, mainly because they are the oldest and best studied group. Significant progress has also been made in the study of metal-metal and rare earth-transition metal alloys, but these developments, although quite important, have not been included. It is shown how the new scattering techniques have confirmed earlier ideas about the high degree of short range order in the metal-metalloid glasses.

In amorphous systems as well as in crystals, atomic transport is governed by structural imperfections. As discussed in the second section, defects in amorphous metals are probably more diffuse than in crystals and can therefore best be described as individual sites with small perturbations of the local short range order.

In the third section this is applied to problems of steady state plastic flow. First, the experiments are reviewed by means of an empirical deformation mechanism map. Then, an attempt is made to describe the basic processes, homogeneous and inhomogeneous flow,

from a unified point of view involving the concentration and motion of individual defect sites that produce local shear. Again, this implies a certain limitation in scope, since significant developments concerning transient flow, anelasticity, internal friction and embrittlement have not been included.

# II. THE STRUCTURE OF TRANSITION METAL-METALLOID ALLOY GLASSES

## 1. Background

Three years ago, around the time of the previous conference, the status of our knowledge about the structure of amorphous metals had been thoroughly reviewed by Cargill.[1,2] Up to that time, information about the atomic scale structure of metal-metalloid alloy glasses derived to some extent from density measurements and indirectly from observations of crystallization and glass transition, but mainly from single wavelength X-ray scattering experiments, which yield radial distribution functions that are dominated by the metal-metal pairs because of the larger concentration and scattering factors of the metal atoms.

These studies had demonstrated conclusively the inadequacy of microcrystalline structural models and the importance of models based on the dense random packing (DRP) of hard spheres. While the DRP of single size spheres was clearly the appropriate model for pure amorphous metals, its suitability for describing the structure of amorphous alloys was still a matter of debate, mainly because of the lack of precise information on the position of the metalloid.

Polk[3] had suggested that the metal atoms form a DRP skeleton, with the metalloids occupying the larger holes in this structure. However, since all these holes, as described by Bernal,[4] are actually too small to accommodate the metalloids, Polk[5] later modified his proposal by appealing to the distortion of the idealized holes in the actual DRP and by allowing, if necessary, some additional relaxation of the hole shape, resulting in a metal skeleton that is less densely packed than the DRP.

The qualitative implications of this model are that a metalloid atom (i) is surrounded by only metal atoms and (ii) has a lower coordination number than a metal atom. The same requirements were the basis of the binary dense random packings by Sadoc et al.,[6] which had, however, limited usefulness for detailed comparison because of the small size of the clusters.

## 2. Recent Experimental Developments

The main experimental advances of the past few years are scattering techniques which yield information about the position and environment of the metalloid atoms. Sadoc and co-workers[7] used neutron, polarized neutron and X-ray scattering to obtain the three partial radial distribution functions for $Co_{81}P_{19}$. They used neutron and X-ray scattering to obtain the Pd-Pd and Pd-Si partial radial distribution functions in $Pd_{84}Si_{16}$ and to establish the absence of Si-Si nearest neighbors. Waseda and co-workers[8] made use of the large anomalous dispersion terms in the X-ray scattering factor for wavelengths near the absorption edge of the scattering element. They applied this in the case of Ni by using Cu K$\alpha$ and Co K$\alpha$ radiation. By combining these data with regular measurements away from the absorption edge (Mo K$\alpha$), they obtained the three partial radial distribution functions for $Ni_{80}P_{20}$. Hayes et al.[9] used the extended X-ray absorption fine structure (EXAFS) of Ge to determine the nearest neighbor environment of this metalloid in $Pd_{78}Ge_{22}$. The nearest neighbor structural data resulting from these investigations are listed in Table 1. For comparison, the same data for crystalline intermetallic compounds of similar compositions are also listed.

TABLE 1: Nearest neighbor structural data for amorphous and crystalline transition metal (Me) - metalloid (X) alloys.

| Composition $Me_{1-x}X_x$ | Metalloid Coordination Number[a] $Z_X$ | Metal Coordination Number[b] $Z_{Me}$ | Average Distance Me-X (Å) | Spread in Me-X Distances (Å) | Average Distance Me-Me (Å) | Metal Goldschmidt Diameter[e] (Å) | Metalloid Radius[f] (Å) | Interstitial Size Ratio[g] | Ref. |
|---|---|---|---|---|---|---|---|---|---|
| Amorphous | | | | | | | | | |
| $Co_{81}P_{19}$ | 8.9 | 12.2 | 2.32 | 0.4 [c] | 2.54 | 2.50 | 1.07 | 0.93 | 7 |
| $Ni_{80}P_{20}$ | 8.5 | 12.9 | 2.35 | 0.6 [c] | 2.55 | 2.49 | 1.10 | 0.94 | 8 |
| $Pd_{84}Si_{16}$ | 9.0 | 12.8 | 2.40 | 0.35 [c] | 2.76 | 2.75 | 1.02 | 0.87 | 7 |
| $Pd_{78}Ge_{22}$ | 8.6 | | 2.486 | <0.2 [d] | | 2.75 | 1.11 | 0.90 | 9 |
| Crystalline | | | | | | | | | |
| $Mn_3P$ | 9 | 13.7 | 2.37 | 0.09 [d] | 2.76 | 2.61 | 1.07 | 0.83 | 11 |
| $Fe_3P$ | 9 | 13.7 | 2.34 | 0.09 [d] | 2.71 | 2.55 | 1.07 | 0.89 | 12 |
| $Ni_3P$ | 9 | 13.7 | 2.29 | 0.10 [d] | 2.68 | 2.49 | 1.04 | 0.89 | 13 |
| $Pd_3Si$ | 8 | 12.7 | 2.44 | 0.19 [d] | 2.90 | 2.75 | 1.06 | 0.85 | 14 |
| DRP Model[h] $Me_{80}X_{20}$ | 8.99 | 12.13 | | | | | | | 31 |

(a) All the neighbors are Me Atoms.

(b) Total coordination number; the number of X neighbors ($Z_{Me}^X$) can be calculated from the composition and the metalloid coordination number: $Z_{Me}^X = xZ_X/(1-x)$.

(c) FWHM; uncorrected.

(d) R.M.S. full width.

(e) From Teatum et al. (10).

(f) The difference between the average Me-X distance and the Me Goldschmidt radius.

(g) For amorphous alloys average Me-X distance/Me Goldschmidt diameter. For crystals: minimum Me-X distance/Me Goldschmidt diameter. (h) relaxed model.

The most important conclusion of these studies is the confirmation of earlier speculation that the degree of chemical short range order in these systems is very high; each metalloid is surrounded by metal atoms only. Comparison with similar crystalline compounds, shows that the metalloid coordination numbers and the average metal-metalloid distance are similar. Besides from analogy with crystalline ordering, the high degree of chemical ordering in the glassy alloys had been anticipated on the basis of model building,[3,5] thermal behavior[15] and composition dependence of some properties,[16] and recently an attempt has been made to explain it in terms of pseudo-potential theory.[17]

The metalloid radius can be estimated by subtracting the metal radius, which for a transition or noble metal is probably close to the Goldschmidt radius, from the average metal-metalloid nearest neighbor distance. The results are listed in Table 1 and illustrated on Figure 1. As had been known for the crystalline materials,[14,18] and had been anticipated for the glasses,[1,15] the observed metalloid radii are smaller than the metalloid Goldschmidt radii. The observed radius for P is close to its tetrahedral covalent radius, as had been pointed out in Rundqvist's review[18] on the crystalline phosphides. The observed radii for Si and Ge in both crystals and glasses, are appreciably smaller than their respective covalent radii. This difference has also been noticed by Rundqvist,[18] but no explanation for it has been offered. It must be concluded that it is difficult to choose a priori an appropriate metalloid radius on chemical grounds. There is probably little significance to the P-radius being close to the tetrahedral covalent one, since recent NMR-measurements[20] on NiP alloys have shown that the binding is metallic in nature.

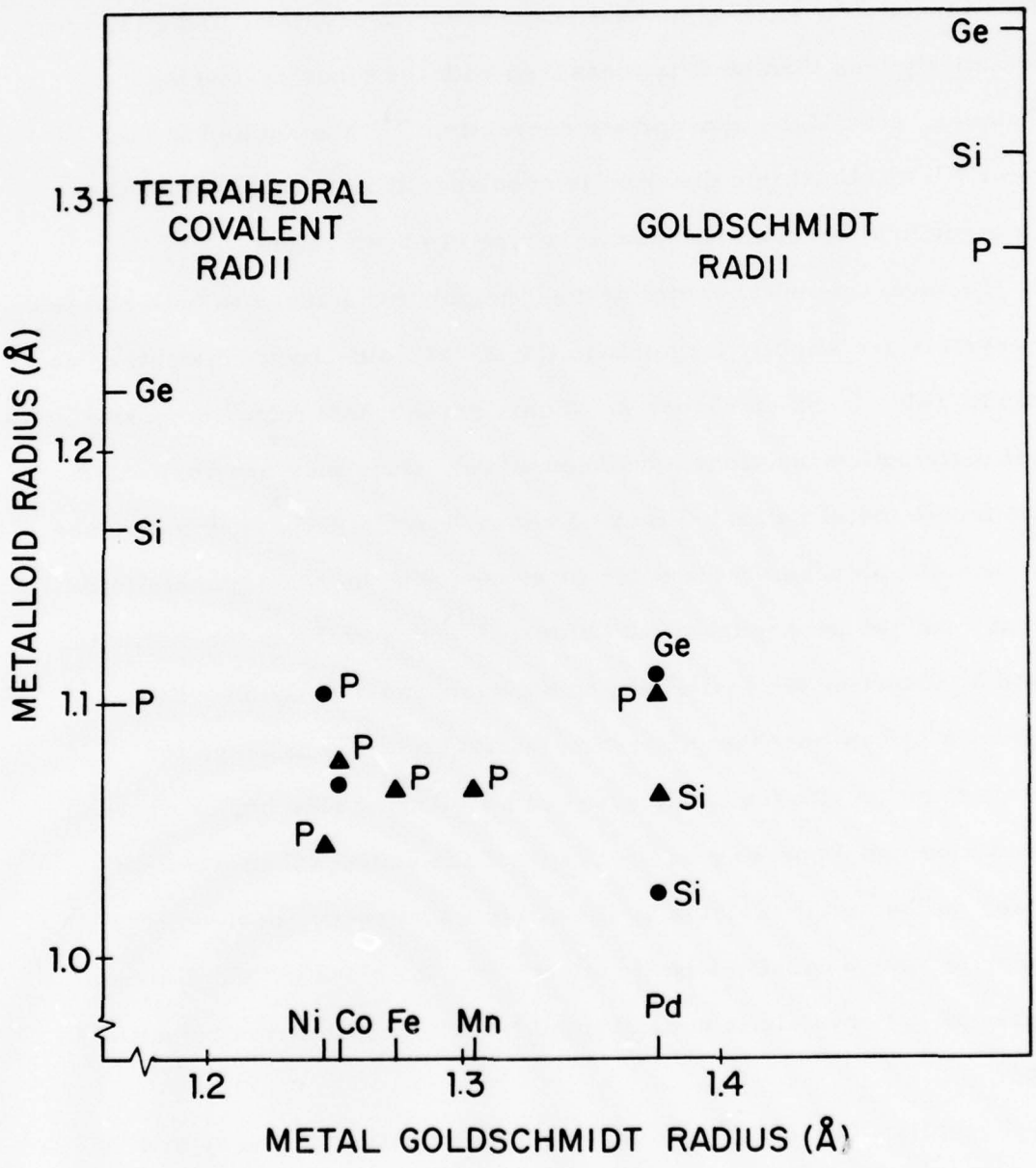


Fig. 1: Metalloid radius vs. Goldschmidt radius for selected glassy (dots) and crystalline (triangles) alloys. Data from Table 1; data for crystalline $Co_2P$ and $Pd_3P$ from Ref. 18; Goldschmidt radii from Ref. 10; covalent radii from Ref. 19.

There seems to be disagreement between the experimental determinations of the spread in metal-metalloid nearest neighbor distances. Using the EXAFS technique, Hayes et al.[9] measure an R. M. S. full width of less than 0.2 Å, similar to what is observed in crystals. This is substantially less than what is measured with the other scattering techniques, even if the appropriate corrections[21] are applied to the listed FWHM. Until this question is resolved, it remains difficult to draw structural conclusions from this type of observations.

The average metal-metal nearest neighbor distances in both glasses and crystals are slightly larger than the metal Goldschmidt diameter, as shown in Table 1 and on Figure 2. (Some earlier data from composite radial distribution functions have been added, since they are dominated by the metal-metal pairs.) Figure 2 shows how the ratio of this distance to the metal Goldschmidt diameter increases with increasing metalloid content. As has been pointed out before,[1,23] this reflects the distortion caused by inserting the metalloids in the pure metal skeleton. It is interesting to note that this distortion is roughly twice as large for crystals than for glasses of the same composition. This higher degree of distortion could possibly be the result of the additional constraints imposed on the metal skeleton by the crystal symmetry requirements. In order to have a density slightly higher than the glasses, the distance increase in the crystals is accompanied by an increase in coordination number.

Recently, Turnbull[24] has analyzed the densities of glassy and crystalline transition metal-metalloid alloys for a large variety of compositions. As illustrated by Figure 3 for the phosphides, he found that the metalloid partial gram-atomic volume $\bar{V}_X$ was equal, within ±10%

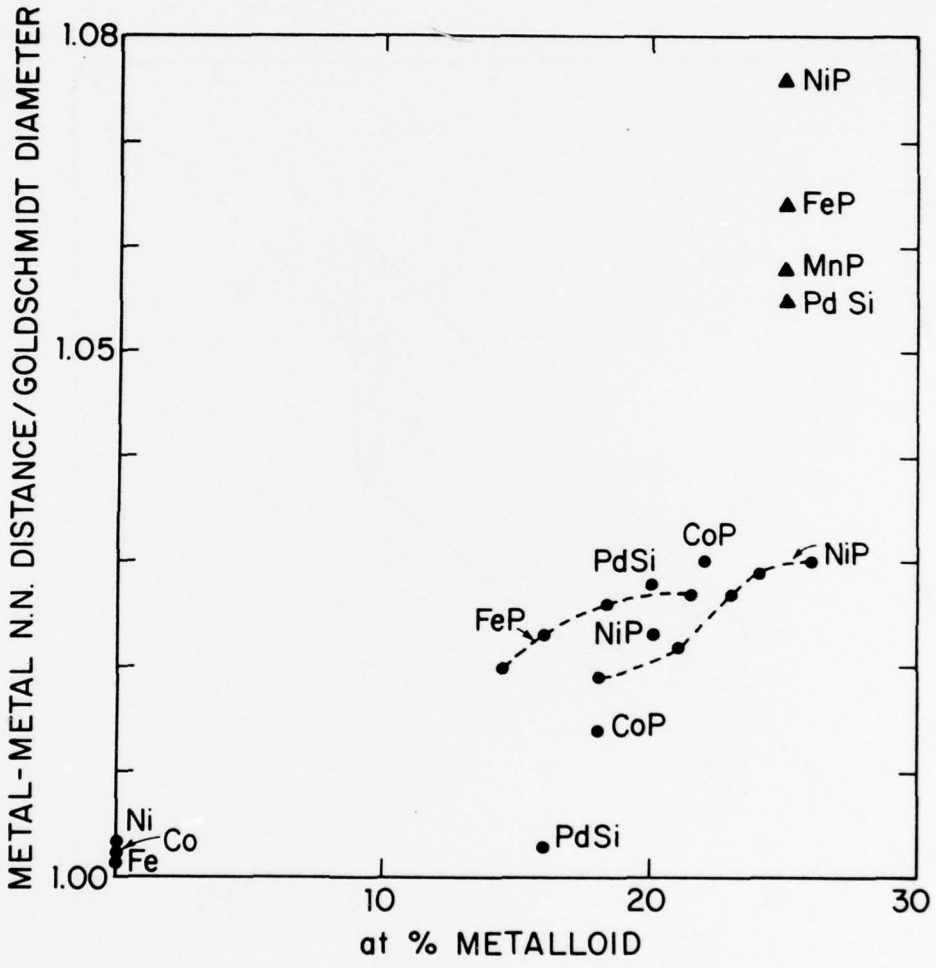


Fig. 2: Change in the ratio of the metal-metal nearest neighbor distance to the metal Goldschmidt diameter with metalloid content. The data for the pure metals, the series of NiP glasses, $Pd_{80}Si_{40}$ and $Co_{80}P_{22}$ are from Cargill's review, ref. 1; the series of FeP glasses is from ref. 22; the rest is from Table 1 (dots: glasses; triangles: crystals).

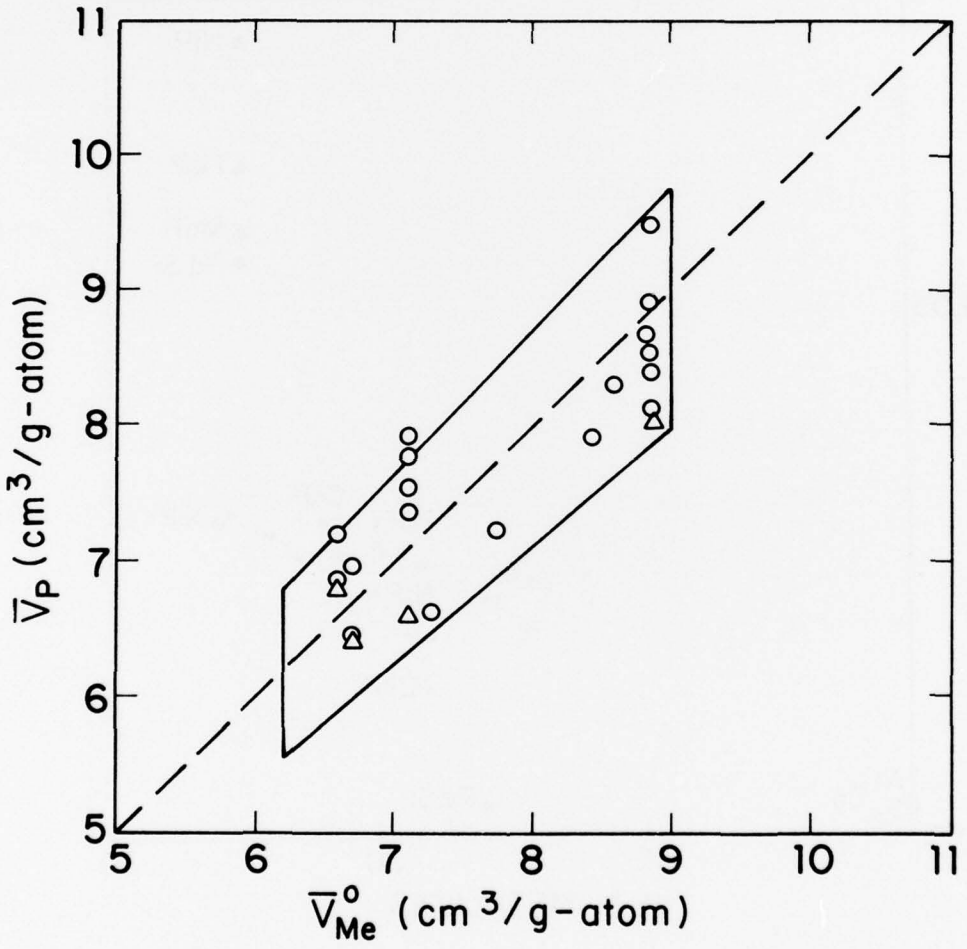


Fig. 3. $\bar{V}_p$: partial gram-atomic volume of P in some glassy (dots) and crystal-line (triangles) Me-P alloys.
$\bar{V}^0_{Me}$: gram-atomic volume of pure Me at 300°K. After Turnbull, ref. 24; some data from ref. 22 have been added.

error limits, to the gram-atomic volume of the pure metal $\bar{V}^0_{Me}$ (which was taken to be equal to $\bar{V}_{Me}$, the partial gram-atomic volume of the metal in the alloy). This scaling relation indicates that the size of the metalloid in these alloys is not an intrinsic property of the element, but is primarily determined by a characteristic spacing in the metal host structure. However, when the observed metalloid radius and the metal Goldschmidt radius are compared (see Fig. 1), the data are scattered and no scaling is apparent. It is possible that a more appropriate choice of size parameters might improve this.

## 3. Recent Model Studies

As discussed above, Polk's[5] reason for modifying his original proposal[3] was that the idealized shapes of the holes that make up Bernal's[4] DRP are too small to accommodate the metalloids. At the time, this was based on analogy with the crystalline metalloid environment. It is confirmed by the measurements of the metal-metalloid distance in the glasses, as shown by the 'interstitial size ratio' in Table 1. This ratio, defined as the metal-metalloid distance over the metal Goldschmidt diameter, is no smaller than 0.87, compared to a center-to-vertex over edge length ratio of 0.82 for the largest idealized hole.[1]

The possibility remained, however, that, since the actual holes in the DRP are distorted (in the sense that their edge lengths can differ by 20%), they could accommodate larger interstitial spheres than the idealized holes. In the light of this possibility, Frost[25] has recently investigated the hole structure of Finney's[26] mechanically built and Bennett's[27] computer-built DRP. He observed that, with spheres within

a fixed cutoff distance being nearest neighbors, these DRP structures cannot be completely described as stacking of the five Bernal polyhedra,[28] but a number of new shapes with four- and five-edged faces have to be included, especially to describe the larger holes. While confirming the predominantly tetrahedral character of the DRP structure, he has obtained statistics for the large holes which are quite different from Bernal's.[4] A similar observation has been made by Whittaker.[45]

For this reason, Frost[25] has made an independent calculation of the exact number and size of all the interstitials in the DRP, without reference to the hole structure. This was done by considering the interstitial spheres in all sets of four DRP spheres (since the center of the largest interstitial sphere is always equidistant between four DRP sphere centers) and eliminating the ones that overlap with a DRP sphere or a larger interstitial. The results are shown in Figure 4. The main conclusion of this study is that, although the holes are distorted in the DRP, they are not appreciably larger than the idealized ones: the largest center to center distance is 0.86 and in order to accommodate 25 interstitials per 100 DRP spheres the interstitial site ratio must be smaller than 0.74. A study of the interstitials in the Bennett DRP led to similar conclusions. Fitting the metalloids of Table 1 in a DRP skeleton, therefore, requires some relaxation of the structure. The remaining question is whether this relaxation involves only local adjustments around the metalloid, or whether it requires a reconstruction of the entire model.

Some insight on this question can probably be obtained from the recent development in constructing dense random packings of binary mixtures of different size spheres. Using the solution of the Percus-Yevick

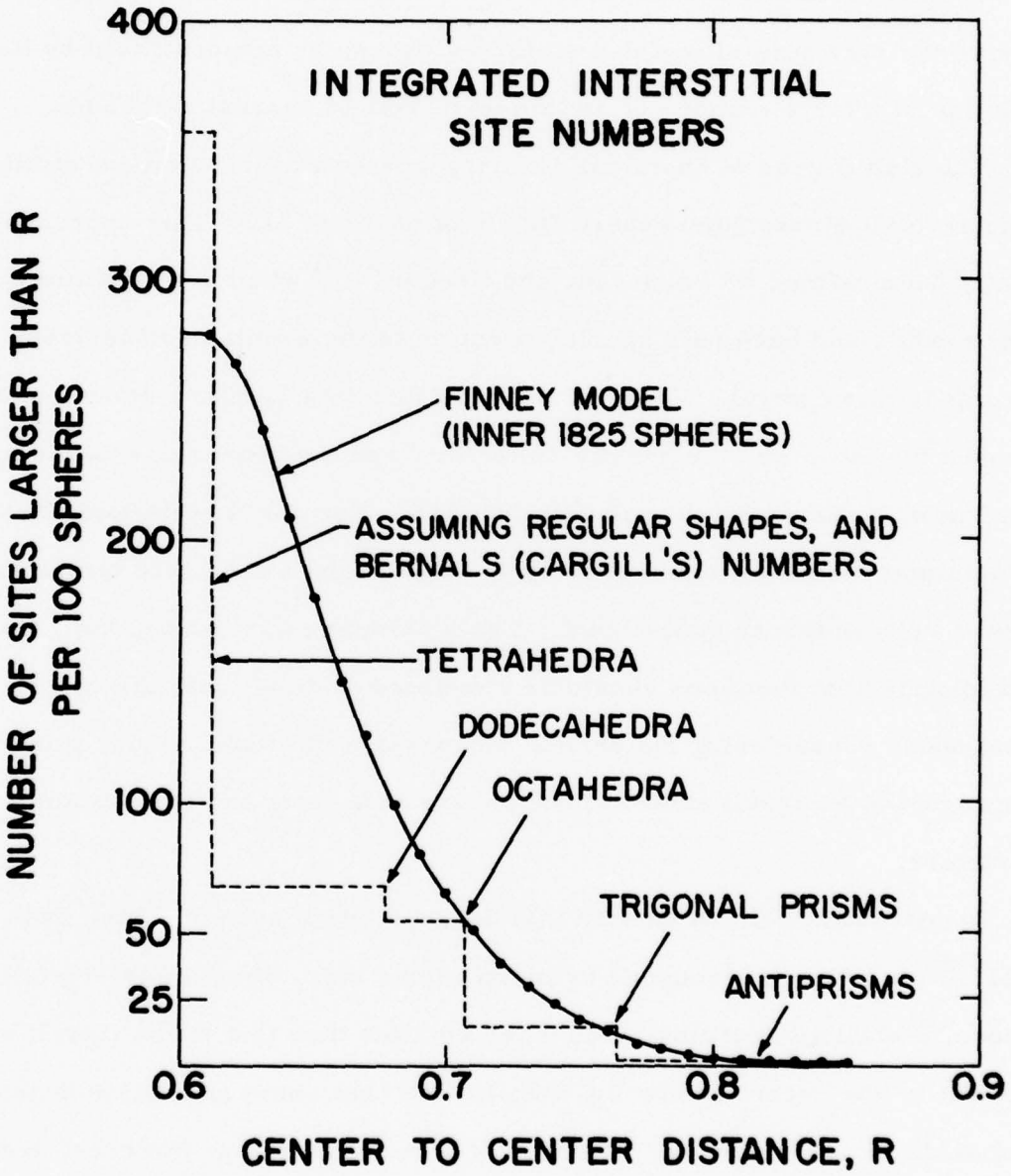


Fig. 4. Interstitial sphere statistics for Finney's[26] DRP, compared to Bernal's[4,1] original statistics. (After Frost, ref. 25). R is the distance between the center of the interstitial sphere and the center of one of the four equidistant nearest DRP spheres. Unit length: DRP sphere diameter.

equation, Weeks[29] has calculated the partial pair correlation functions for a number of binary hard sphere mixtures with various compositions and sphere size ratios. This approach however fails to take into account the chemical interaction between the two kinds of atoms. This makes it inappropriate to describe the structure of metal-metalloid glasses, as demonstrated by its prediction of a large number of metalloid-metalloid nearest neighbors.

The high degree of chemical ordering was an explicit element of the computer-built binary hard sphere DRP's of Sadoc et al.[6] This approach has recently been refined by Boudreaux and Gregor[30, 31] who have built much larger models and have paid special attention to the problems of isotropy and composition control. Relaxing the structure in a Lennard-Jones potential improved the isotropy, the density uniformity and the appearance of the split second peak in the radial distribution function. For a 20% metalloid alloy[31] they obtained coordination numbers (see Table 1) and a structure factor that compare very well with experiment. For a complete evaluation, their partial radial distribution functions should be compared in detail with the experimental ones. Considering the earlier discussions of atomic sizes, this probably requires a careful choice of the sphere size ratio and the potential parameters.

In conclusion, it can be said that the qualitative aspects of the Polk model[3, 5] (metalloid surrounded by metal atoms only, short metal-metalloid distance, metalloid coordination number smaller than that of the metal) are borne out by the recent scattering studies, but that some relaxation of the metal skeleton is necessary. The idea of a metal skeleton, however, besides being quite elegant, remains an attractive one in the light of Turnbull's scaling relation.[24] It would therefore be interesting to check whether the hole structure formed by the metal atoms in the binary DRP's can be related simply to that of the single atom DRP.

type of TSRO and this tends to keep defects localized. In an amorphous structure, this requirement is relaxed and therefore a variety of TSRO types can be accommodated. Because of this flexibility, it seems that localized point, line and planar defects are not likely to occur as such in amorphous systems, but probably become diffuse by breaking up in small perturbations of the TSRO over an extended region. This has indeed been observed for artificially created "vacancies" in two-,[43] and three-dimensional[44] amorphous model systems.

Based on positron-annihilation[47] studies of cold rolled metallic glasses, the same can probably be expected for a line defect. The analogue of a localized crystalline dislocation created instantaneously in an amorphous model system would probably be unstable. Not only would its core become very diffuse, but the displacements and climb resulting from its interaction with local stress fields and partial vacancies would lead to a dislocation line that is contorted on an atomic scale. Since under the influence of an external stress these segments will move in an uncorrelated way, the resulting deformation process should be thought of as one governed by the motion of individual defect sites rather than by glide of a dislocation line.

The most fruitful way to describe structural defects in amorphous systems, therefore, is as individual sites where the 'ideal' or preferred local SRO is perturbed. In general they include both deviations from the ideal CSRO (i.e., wrong nearest neighbors) or ideal TSRO (e.g., the last configuration in Fig. 5, which has probably a higher energy than the first one). The presence of non-ideal SRO facilitates structural rearrangements at these sites, since it lowers the energy difference

between the initial and activated state of the rearrangement process. The various atomic transport processes (diffusion, volume relaxation, flow) are therefore governed by the concentration and mobility of these defects.

It has been suggested[43] that the large differences that have been observed[46] between the time constants of some of the atomic transport processes can be explained by distinguising between different types of defects depending on the type of rearrangement they allow (nearest-neighbor change → diffusion; long range stress field → volume relaxation; local shear → flow).

# IV. STEADY STATE PLASTIC FLOW

## 1. Survey of the Experiments

A convenient way of summarizing the flow data for a material is by means of an empirical deformation mechanism map:[48] each point on the map represents an experiment at constant stress ($\tau$) and temperature (T), and contours are drawn connecting points of the same steady strain rate ($\dot{\gamma}$). Figure 6 is an example for Pd-based glasses. Data obtained from compression[37-39] and creep tests[32, 35], or measurements of the ultimate tensile strength (the three highest points of Ref. 33) are probably close to the steady state values. For all the other tests the fracture stress, which in most of these cases coincides with the yield stress, has been plotted. It is probably too low, since steady state flow has been forestalled by fracture. If more--and more consistent--data, or complete constitutive equations were available, the resulting deformation mechanism map would probably resemble the schematic one of Fig. 7. It is included here to illustrate the basic modes of deformation: homogeneous and inhomogeneous flow.

### (a) Homogeneous Flow

In this type of flow each volume element of the specimen contributes to the strain. In a uniaxial tensile test, fracture occurs at large strains and after extensive necking. This flow mechanism operates at low stress levels at all temperatures and is, except near the boundary of the inhomogeneous flow region, almost always a Newtonian viscous (i.e., $\dot{\gamma} \propto \tau$). For this reason the shape of the strain rate contours

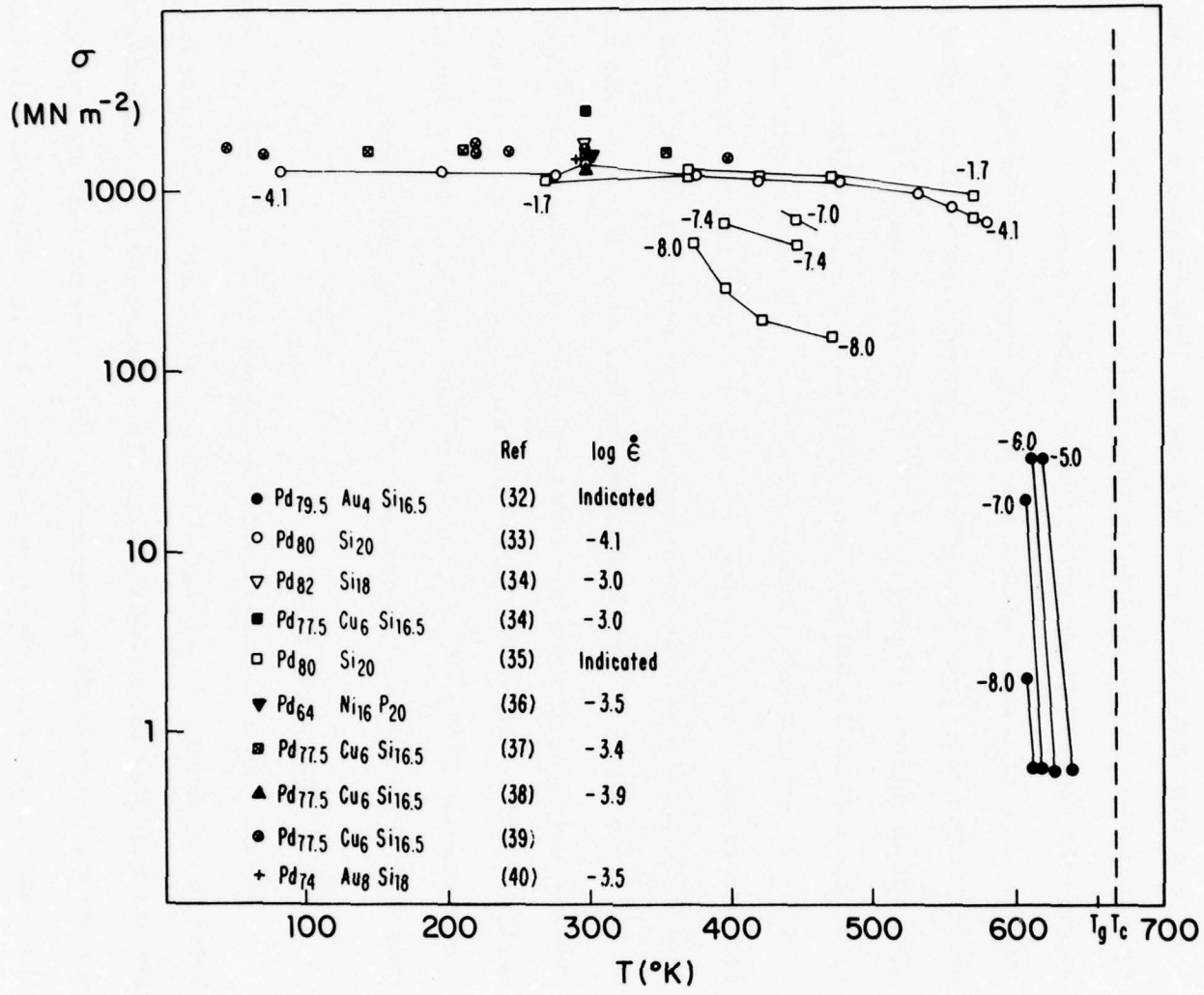


Fig. 6. Empirical deformation mechanism map for Pd-based glasses. Stress ($\sigma$) and strain rate ($\dot{\epsilon}$) are uniaxial. $T_g$ and $T_c$ for $Pd_{80}Si_{20}$. After ref. 49.

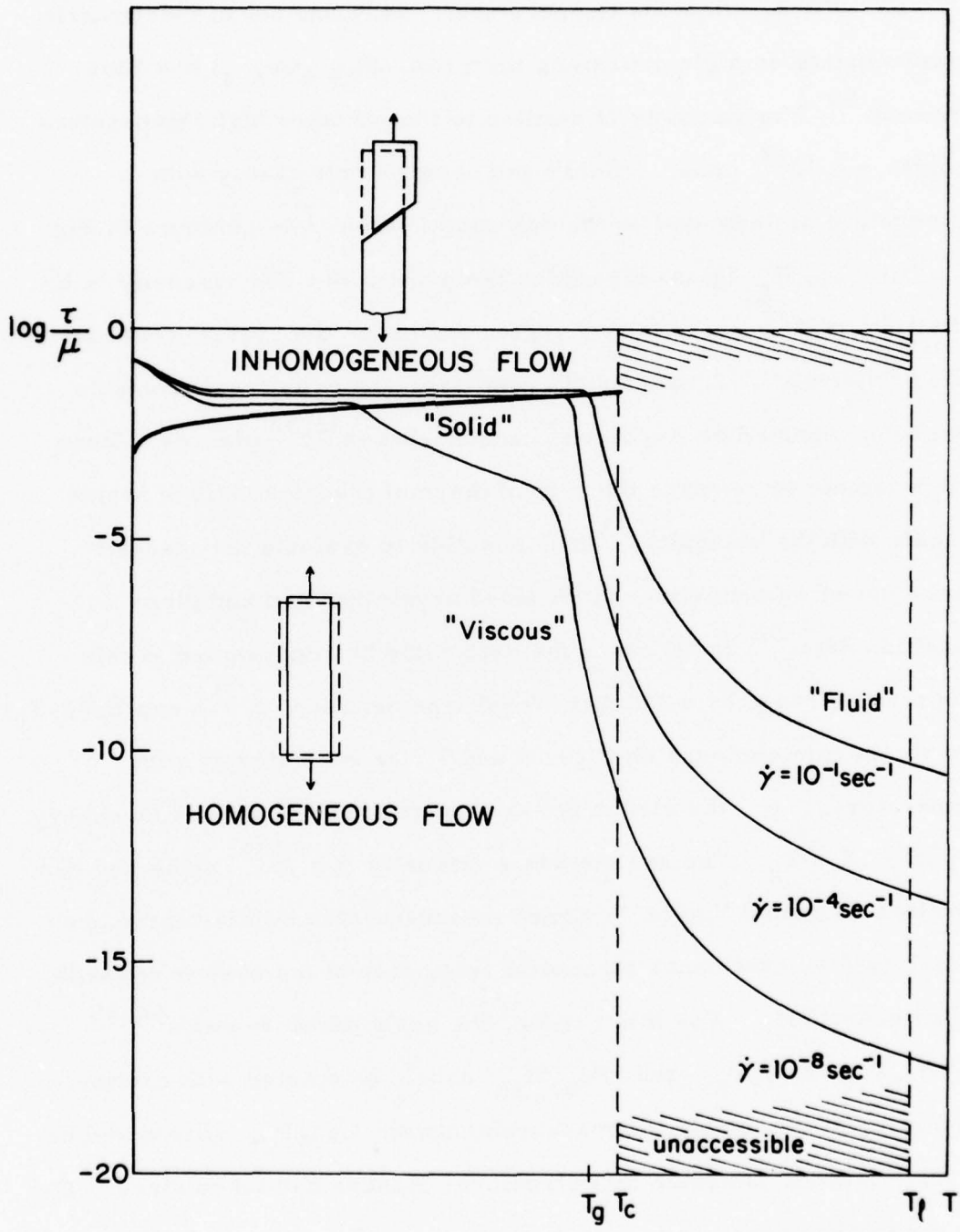


Fig. 7. Schematic deformation mechanism map for a metallic glass illustrating the basic modes of deformation. From ref. 49.

reflects that of the viscosity--temperature curve.[43] Three, somewhat arbitrarily defined, regions can be distinguished:

(i) $T > T_\ell$ (liquidus temperature). Only one set of viscometric measurements on a glass forming melt ($Au_{77}Si_{13.6}Ge_{9.4}$) has been reported.[50] The viscosity is similar to that of other high temperature liquids: $\eta \approx 10^{-2}$ poise, ('fluid') and changes only slowly with temperature as indicated by the horizontal strain rate contours in Fig. 7.

(ii) $T \approx T_g$ (glass transition temperature). The viscosity is by definition $\sim 10^{13}$ poise in this region and hence the system could be called "viscous". A number of creep-type viscosity measurements have been reported on Au-based[51] and Pd-based[32,52] glasses. Since in this temperature range the rate of thermal transformations seems to scale with the viscosity,[53] it is possible to evaluate the viscosity from a set of calorimetrically obtained crystallization and glass transition data.[52] In all cases the data could be represented in this temperature range by a Fulcher-Vogel type equation: $\eta = A \exp[B/(T-T_0)]$. The strain rate contours on Figs. 6 and 7 rise very steeply with temperature, i.e., the viscosity has a large apparent activation energy.

(iii) $T < T_g$. The system has a viscosity $\eta > 10^{15}$ poise and can therefore be called "solid." Creep measurements in this region are complicated by continuous structural relaxation of the system towards higher viscosities. For this reason, the early measurements[54,35] on $Ni_{75}P_{25}$, $Co_{75}P_{25}$ and $Pd_{80}Si_{20}$ should be treated with caution. For example, rerunning the measurements on $Co_{75}P_{25}$ gave a higher viscosity, which indicated that structural changes had taken place. The low activation energy observed for $Pd_{80}Si_{20}$ (0.6 eV) might also

increase up annealing, as indicated by the diffusion measurements on a similar system.[46] In order to perform a truly iso-configurational creep test it is necessary to anneal the specimen for a long time at a temperature higher than that of the test, as demonstrated by Hadnagy et al.[55] in their load relaxation studies of a $Fe_{40}Ni_{40}P_{14}B_6$ glass. They found that the plastic flow component of the relaxation had a strain rate sensitivity exponent ($m = \partial \ln \dot{\gamma} / \partial \ln \tau$) of about 4. This is larger than what had been measured earlier[35, 54] ($m \approx 1$), but similar to Megusar et al.'s recent observations[56] on $Pd_{80}Si_{20}$ ($4 < m < 10$).

(b) Inhomogeneous Flow

This type of flow, in which the strain is localized in a few very thin shear bands, operates at high stress levels. (See Fig. 7) In this region, the strain rate contours are very close together, i.e., the strain rate is very stress sensitive (the exponent m is large). The flow stress is almost temperature independent, except for an upturn at low temperatures especially in Fe- and Ni-based glasses.[61, 62] Recent direct observations of the shear bands have shown that they are $\sim$50 Å thick[57] and form very rapidly[58] (< 6.7 msec) prior to fracture. Although the specimen's total plastic strain is quite small (< 0.2%), the local plastic strain in the shear bands is very large. This causes the local cross section of the specimen to decrease until the stress concentration is large enough to induce fracture along the shear plane by the Taylor instability mechanism,[59, 60] which produces a vein-like pattern on the fracture surface.

It seems clear from a number of considerations that this inhomogeneous flow phenomenon must involve a structural change which

produces a local softening (i.e., lowering of the viscosity) in the shear band: (i) such a change would obviously confine all shear to the band; (ii) the shear bands occur, depending on the specimen geometry, at different angles with the tensile axis but are never normal to it; since fracture occurs along the shear band rather than normal to the tensile axis indicates that the band has been weakened; (iii) differential etching[63,64] and small changes in the diffraction pattern[65] have been observed.

## 2. Microscopic Models

### (a) Defect-Free Flow: The Ideal Shear Strength

The ideal shear strength ($\tau_{id}$) is the stress at which the structure becomes unstable: it shears off over its whole cross-section at once. The simple Frenkel calculation,[66] which assumes a sinusoidal shape for the potential curve, yields $\tau_{id} = \mu/2\pi$ ($\mu$: shear modulus). It is probably more appropriate for amorphous solids, which are mechanically isotropic, then for crystals, where subsidiary minima in the potential curve corresponding to the easiest glide directions tend to give a lower value for $\tau_{id}$.

### (b) Defect Controlled Flow

(i) The General Flow Equation. As discussed in the previous section, atomic transport processes are governed by the concentration and motion of the appropriate type of defect. In the case of plastic flow this defect is a site of volume $v_0$, which upon rearrangement produces a local shear strain $\gamma_0$. It is easy to show that the macroscopic strain rate can, quite generally, be expressed as:

$$\dot{\gamma} = n v_0 \gamma_0 k_0 \qquad (1)$$

where $n$ is the concentration of defect sites and $k_0$ the frequency of rearrangement at a site. Chemical rate theory[67,68] gives an expression for $k_0$ of the form:

$$k_0 = \nu_D \exp\left(-\frac{\Delta G'}{kT}\right) \sinh\left(\frac{\tau \gamma_0 v_0}{kT}\right) \qquad (2)$$

The hyperbolic sine is the stress-dependent driving factor and $\Delta G'$ is the activation free energy for rearrangement, which, in general, contains chemical and strain energy contributions. $\nu_D$ is the frequency of atomic vibration ($\sim$ Debye frequency).

Expressions of the type of eq. (1) have been used for a long time to describe flow[68] and are general enough to include the case of dislocation glide in crystals. For example, in a simple cubic lattice (lattice parameter a), $n = \rho/\ell$ ($\rho$: dislocation density; $\ell$: average dislocation length), $v_0 = a^2\ell$, $\gamma_0 = b/a$ (b: Burgers vector), $k_0 = v/a$ (v: dislocation velocity). Equation (1) then becomes $\dot{\gamma} = \rho b v$, the Orowan equation. Based on the macroscopic analogy between the surface steps produced by the shear bands in amorphous metals and the slip bands formed during plastic deformation of crystals, a number of workers[69-71] have invoked the presence of localized dislocation lines to explain inhomogeneous flow. Subsequent investigations,[47] however, have failed to produce evidence for their existence and it will be shown later on that the formation shear bands can be explained as a macroscopic instability effect, without recourse to dislocation lines. The present approach, based on local shear produced by individual defect

sites, is more consistent with the structural observations and provides a more unified view of the deformation process since it applies to both homogeneous and inhomogeneous flow.

(ii) Homogeneous Flow, $T > T_\ell$ ('Fluid'). An adequate characterization of the viscosity of liquids at high temperatures has been available for a long time.[67, 72] The mechanism involves switching of individual atoms ($v_0 \approx$ atomic volume $\Omega$, $\gamma_0 \approx 1$). The number of defect sites is of the same order of magnitude as the number of atoms and therefore changes little with temperature. For the low stress levels of fluid flow: $\sinh(\tau\gamma_0 v_0/kT) \approx \tau\gamma_0 v_0/kT$, i.e.: the flow is Newtonian. The activation free energy $\Delta G'$ is very small, probably because at these high defect concentrations the structure is flexible enough to make the elastic energy involved in switching negligible. For this reason the temperature dependence of the viscosity is small.

(iii) Homogeneous Flow, $T \approx T_g$ ('Viscous'). In this region the change of $\dot{\gamma}$ with temperature is dominated by the defect concentration n. The SRO in the system increases rapidly with decreasing temperature, and this causes a corresponding decrease of the defect concentration.

In the free volume theory, developed by Turnbull and Cohen[73] for monatomic systems, a defect site is defined as a local density fluctuation which creates a hole large enough to allow a neighboring atom to jump into it (i.e., $v_0 \approx \Omega$, $\gamma_0 \approx 1$). The defect concentration is then

$$n = \left(\frac{1}{\Omega}\right) \exp\left(-\frac{\gamma' v^*}{v_f}\right). \qquad (3)$$

where $\gamma'$ is a geometrical overlap factor of order unity, $v^*$ the minimum hole size ($\sim$ ion core volume for metals) and $v_f$ the average free volume per atom (defined as the difference between the actual atomic volume ($\Omega$) and that of a reference system with ideal SRO ($\Omega_0$); the reference system for hard spheres is the DRP). At constant pressure, the average free volume can be expressed as $v_f = \alpha(T-T_0)\Omega_0$, where $\alpha$ is an average coefficient of thermal expansion and $T_0$ the equilibrium temperature of the reference system. Combined with eq. (3), which is the dominating term in eq. (1), this leads to a Fulcher-Vogel type expression for the viscosity.

Since $\alpha$ is not a constant, however, and measurements of it are rarely available, theoretical calculations of the thermal expansion are useful. This has been done by Ramachandrarao et al.,[74] who used the hole theory of liquids to derive an expression for $v_f$ which varies exponentially with inverse temperature. This allowed them to fit the viscosity data for a member of glassforming melts over the entire temperature range $T_\ell - T_g$, something which cannot be done with a single Fulcher-Vogel expression.

An alternative approach to the calculation of the defect concentration is the configurational entropy model of Adam and Gibbs,[75] in which a defect site is defined as a subsystem with a configurational entropy exceeding some critical value $S_c^*$. Chen[76] has applied this model to the flow of glassy metals. It appears[77] that under certain conditions the two models should reduce to the same form. The configurational entropy approach, however, is more phenomenological in nature and does not seem to provide as much insight into the atomistic details of the local shear mechanism as the free volume model does.

Since the free volume model implies $v_0\ \gamma_0 \approx \Omega$ one would expect that at the experimental stress levels $\sinh(\tau\ v_0\ \gamma_0/kT) \approx \tau v_0 \gamma_0/kT$ and that the flow would be Newtonian. Chen and Goldstein's measurements[32] on $Pd_{77.5}Cu_6Si_{16.5}$ glasses confirm this for high viscosities ($10^{12}$ - $10^{13}$ poise), but at lower viscosities ($10^{11}$ - $10^{12}$ poise) they report non-Newtonian behavior, corresponding to a value of $v_0\ \gamma_0$ as high as $100\Omega$. This result seems somewhat inconsistent in view of the Newtonian behavior at both lower and higher viscosities, and it remains as yet unexplained.

(iv) Homogeneous Flow, $T < T_g$ ('Solid'). In order to perform meaningful measurements in this region it is necessary to stabilize the structure by annealing. Since such a system is frozen in one particular configuration, one might at first expect that according to the free volume model the defect concentration would remain constant at the level defined by the fictive temperature. However, it should be realized that even in a frozen-in configuration, $v_f$ still decreases with decreasing temperature because of the non-configurational (i.e., uniform) part of the thermal expansion. At the same time $v^*$ increases because of the increasing effective hard core diameter of the metal ion (defined[78] as the distance at which the repulsive potential energy is $kT$ above the minimum). Equation (3) shows that these two effects result in a continued decrease in defect concentration with decreasing temperature. Combined with a contribution from $\Delta G'$, which in this model is mainly chemical in origin, this would predict a fairly large observed activation energy for the iso-configurational viscosity. Such data are not available yet, but the large activation energy observed in diffusion measurements[46] on annealed specimens points in the same direction.

Recently, Argon[79] has proposed a somewhat different approach to this type of flow. In the three volume description the defect concentration is small ($n < 10^{-15}/\Omega$), but the rearrangement at each site is relatively easy ($\Delta G'$ contains only a chemical contribution). In Argon's model, the defect sites are larger ($v_0 \approx 50\,\Omega$) but the local shear strain is smaller ($\gamma_0 \approx 0.1$); the defect concentration is larger ($n\, v_0 \approx 1$) but the rearrangements are more difficult ($\Delta G'$ contains an elastic strain energy and a shear resistance term). The qualitative results from the two models are therefore likely to be similar.

The models differ quantitatively in their predictions of the strain rate sensitivity exponent. From eq. (1) and (2) follows:

$$m = \frac{\partial \ln \dot{\gamma}}{\partial \ln \tau} = \left(\frac{\tau\, \gamma_0\, v_0}{kT}\right) \coth\left(\frac{\tau\, \gamma_0\, v_0}{kT}\right) \qquad (4)$$

Observations have been made for stresses around $\tau = 5 \times 10^8 Nm^{-2}$ and $T = 500K$. Argon's model ($\gamma_0\, v_0 \approx 5$) predicts $m \approx 5$, in accordance with the observations. The free volume model ($\gamma_0 v_0 \approx 1$) predicts $m = 1$, and needs therefore some generalization which allows the rearrangement of more atoms per defect site.

(v) Inhomogeneous Flow. As discussed above, formation of the shear bands involves a structural change that leads to a lowering of the viscosity in the band. In the free volume model, the viscosity is governed by the defect concentration, and hence a decrease in viscosity must correspond to an increase in the average free volume $v_f$. Following a general suggestion by Polk and Turnbull,[50] Spaepen[49] has shown that at high stress levels the free volume in the band is increased as a result of a dynamic equilibrium between stress-driven creation of

free volume (atoms pushing their neighbors aside) and its annihilation by diffusional rearrangements (the system tries to relax back to its original state). The resulting expression for the defect concentration does not depend on the original structure, but is a strong function of the stress and the diffusion rate:

$$\ln n = - \frac{S v^*}{2kTn_D} \left[ \cosh\left(\frac{\tau \Omega}{2kT}\right) - 1 \right]^{-1} \qquad (5)$$

where $S = 2\mu(1+\nu)/3(1-\nu)$ and $n_D$ the number of jumps necessary to annihilate an amount of free volume equal to $v^*$ $(1 < n_D < 10)$.

The model can predict the boundary line between the homogeneous and inhomogeneous flow regions (see Fig. 8) in terms of reasonable physical parameters. Since the defect concentration n is the dominant term in eq. (1) and a strong function of the stress, the model predicts a very large strain rate sensitivity coefficient m, in accordance with observations. An estimate of m can easily be made by differentiating eq. (5) as a function of $\ln \tau$. Insertion of typical values ($S = 5.12 \times 10^{10}$ $Nm^{-2}$, $\tau = 6 \times 10^8 Nm^{-2}$, $\Omega = 1.4 \times 10^{-29} m^3$, $v^*/n_D = 0.26\Omega$, $T = 300K$) yields $m = 85$.

Argon[79] has recently applied this idea to a model involving "small dislocation loop-like" defect sites ($v_0 \approx 20\Omega$, $\gamma_0 = 1$). In his model the free volume affects the viscosity by lowering the shear resistance term in $\Delta G'$. It predicts the homogeneous-inhomogeneous transition, but the idea of a "small dislocation loop" should not, for topological reasons, be taken to literally. More importantly, however, his analysis shows rigorously that localization of the shear in bands is a direct result of the softening caused by the dynamic excess of free volume.

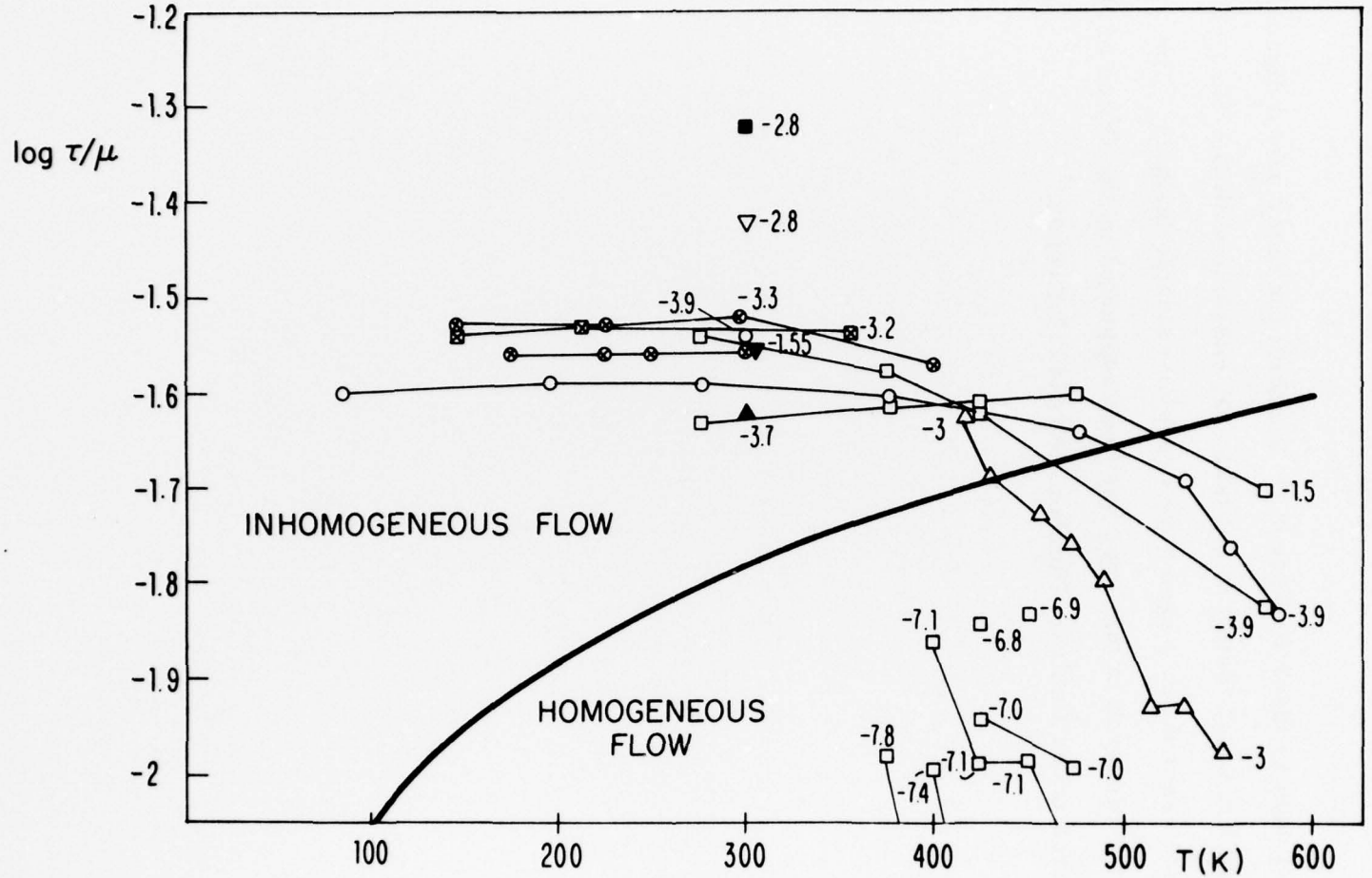


Fig. 8. Enlarged portion of Fig. 6 (normalized). Δ: yield stress is for $Pd_{80}Si_{20}$ from ref. 56. The heavy line is the boundary between regions of homogeneous and inhomogeneous flow, calculated in ref. 49.

## ACKNOWLEDGEMENTS

I want to thank Professor D. Turnbull for many useful discussions and for a critical review of the text. Discussions with Dr. H. J. Frost and Professor A. S. Argon have provided valuable insights. The author's research in this area has been supported by the Office of Naval Research under Contract Number N00014-77-C-0002.

## REFERENCES


1. G. S. Cargill III, Solid State Physics, 30, (F. Seitz, D. Turnbull and H. Ehrenreich, eds.), p. 227, (1975), Academic Press, N. Y.

2. G. S. Cargill III, Proc. 2nd Int. Conf. on Rapidly Quenched Metals (N. J. Grant and B. C. Giessen, eds.), p. 293, (1976), M. I. T. Press, Cambridge, MA.

3. D. E. Polk, Scripta Met., (1970), 4, 117.

4. J. D. Bernal, Proc. Roy. Soc., (1964), A280, 299.

5. D. E. Polk, Acta Met., (1972), 20, 485.

6. J. F. Sadoc, J. Dixmier and A. Guinier, J. Non-Cryst. Solids, (1973), 12, 46.

7. J. F. Sadoc, Thesis, (1976), University of Paris.

8. Y. Waseda, H. Okazaki, M. Naka and T. Masumoto, Sci. Rep. Res. Inst. Tohuku Univ., (1976), 26A, 12. The data have been taken from a review paper, ref. 23.

9. T. M. Hayes, J. W. Allen, J. Tauc, B. C. Giessen and J. J. Hauser, Phys. Rev. Letters, (1978), 40, 1282.

10. E. Teatum, K. Gschneidner and J. Waber, LA-2345, (1960), U. S. Dept. of Commerce, Washington, D. C. Listed by W. B. Pearson, "The Crystal Chemistry and Physics of Metals and Alloys," p. 151, (1972), Wiley, N. Y.

11. S. Rundqvist, Acta Chem. Scand., (1962), 16, 995.

12. S. Rundqvist, Acta Chem. Scand., (1962), 16, 10.

13. S. Rundqvist, Acta Chem. Scand., (1962), 16, 242.

14. B. Aronsson, Ark. Kemi., (1960), 16, 379.

15. D. Turnbull, J. de Physique, (1974), 35, C-4, 1-49.

16. H. S. Chen and B. K. Park, Acta Met., (1973), 21, 395.

17. S. R. Nagel and J. Tauc, Solid St. Comm., (1977), 21, 129.

18. S. Rundqvist, Ark. Kemi., (1962), 20, 67.

19. L. Pauling, "Nature of the Chemical Bond," 3rd ed., p. 224, (1960), Cornell University Press, Ithaca, N. Y.

20. L. H. Bennett, H. E. Schone and P. Gustafson, "Nuclear Magnetic Resonance Studies of Amorphous Ni-P Alloys," (1978), to be published.

21. See G. S. Cargill, ref. 1, p. 242.

22. J. Logan, Phys. Stat. Sol. (a), (1975), 32, 361.

23. Y. Waseda, H. Okazaki and T. Masumoto, J. Mat. Sci., (1977), 12, 1927.

24. D. Turnbull, Scripta Met., (1977), 11, 1131.

25. H. J. Frost, "Hole Statistics in Dense Random Packings," (1978), submitted to Acta Met.

26. J. L. Finney, Proc. Roy. Soc., (1970), 319A, 479.

27. C. H. Bennett, J. Appl. Phys., (1972), 43, 2727.

28. There has been some confusion on the nature of the polyhedra that make up the DRP. In his original paper (J. D. Bernal, Nature, (1960), 185, 68) Bernal claims that the DRP is made up of 5 basic polyhedra (tetrahedra, half-octahedra, dodecahedra, trigonal prisms and archimedian antiprisms). Notice that three of these polyhedra have four-edged faces and Bernal states specifically that they can join by these faces. His accompanying figure, however, shows these polyhedra with half-octahedral caps on all four-edged faces, thus creating deltahedra (i.e., polyhedra with triangular faces). Some workers[5, 23] have read this to mean that the entire DRP could be made up of these 5 basic deltahedra which was, in fact, not Bernal's original claim. Frost[25] has also checked this possibility and has determined that, with his nearest neighbor definition, the DRP cannot be described as a stacking of only these five deltahedra, but that a substantial volume fraction is taken up by large, contorted deltahedra. It is possible, however, that with a more flexible nearest neighbor definition these large deltahedra could be broken up in terms of the small ones.

29. J. D. Weeks, Phil. Mag., (1977), 35, 1345.

30. D. S. Boudreaux and J. M. Gregor, J. Appl. Phys., (1977), 48, 152.

31. D. S. Boudreaux and J. M. Gregor, J. Appl. Phys., (1977), 48, 5057.

32. H. S. Chen and M. Goldstein, J. Appl. Phys., (1971), 43, 1642.

33. T. Masumoto and R. Maddin, Acta Met., (1971), 19, 725.

34. H. J. Leamy, H. S. Chen and T. T. Wang, Met. Trans., (1972), 3, 699.

35. R. Maddin and T. Masumoto, Mat. Sci. Eng., (1972), 9, 153.

36. H. S. Chen, Scripta Met., (1973), 7, 931.

37. C. A. Pampillo and H. S. Chen, Mat. Sci. Eng., (1974), 13, 181.

38. H. S. Chen and D. E. Polk, J. Non-Cryst. Solids, (1974), 15, 174.

39. C. A. Pampillo, J. Mat. Sci., (1975), 10, 1194.

40. C. P. Chou and F. Spaepen, Acta Met., (1975), 23, 609.

41. H. J. Frost, private communication.

42. F. Spaepen and D. Turnbull, Proc. 2nd Int. Conf. on Rapidly Quenched Metals (N. J. Grant and B. C. Giessen, eds.), p. 205, (1976), M.I.T. Press, Cambridge, MA.

43. F. Spaepen, "Structural Imperfections in Amorphous Metals," (1978), to be published J. Non-Cryst. Solids.

44. P. Chaudhari, private communication.

45. E. J. W. Whittaker, N. Non-Cryst. Solids, (1978), 28, 293.

46. A large difference between the time constant for diffusion and volume relaxation has been observed by H. S. Chen, L. C. Kimerling, J. M. Poate and W. L. Brown, Appl. Phys. Lett., (1978), 32, 461.

47. H. S. Chen and S. Y. Chuang, J. Electr. Mater., (1975), 4, 783.

48. Detailed discussion in H. J. Frost and M. F. Ashby, Proc. J. E. Dorn Symp. (J. C. M. Li and A. K. Mukherjee, eds.), p. 70, (1975), A.S.M., Cleveland, Ohio; M. F. Ashby and H. J. Frost, "Constitutive Equations in Plasticity," (A. S. Argon, ed.), p. 117, (1975), M.I.T. Press, Cambridge, MA.

49. F. Spaepen, Acta Met., (1977), 25, 407.

50. D. E. Polk and D. Turnbull, Acta Met., (1972), 20, 493.

51. H. S. Chen and D. Turnbull, J. Chem. Phys., (1968), 48, 2560.

52. H. S. Chen, J. Non-Cryst. Solids, (1978), 27, 257.

53. F. Spaepen and D. Turnbull, in "Metallic Glasses," p. 114, (1977), A.S.M., Cleveland, Ohio.

54. J. Logan and M. F. Ashby, Acta Met., (1974), 22, 1047.

55. T. D. Hadnagy, D. J. Krenitsky, D. G. Ast and C.-Y. Li, Scripta Met., (1978), 12, 45.

56. J. Megusar, N. J. Grant and A. S. Argon, (1978), to be published in these conference proceedings.

57. K. V. Sethi, R. Gibala and A. H. Heuer, Scripta Met., (1978), 12, 207.

58. H. Neuhauser, Scripta Met., (1978), 12, 471.

59. F. Spaepen, Acta Met., (1975), 23, 615.

60. A. S. Argon and M. Salama, Mat. Sci. Eng., (1976), 23, 219.

61. D. J. Krenitsky and D. G. Ast, "Temperature dependence of the flow stress and ductility of annealed and unannealed amorphous $Fe_{40}Ni_{40}P_{14}B_6$," (1978), Report No. 2950, Cornell Materials Science Center.

62. C. A. Pampillo and D. E. Polk, Acta Met., (1974), 22, 741.

63. C. A. Pampillo, Scripta Met., (1972), 6, 915.

64. S. Takayama and R. Maddin, Acta Met. (1975), 23, 943.

65. T. Masumoto, H. Kimura, A. Inoue and Y. Waseda, Mat. Sci. Eng., (1976), 23, 141.

66. J. Frenkel, Z. Phys., (1926), 37, 572.

67. S. Glasstone, K. J. Laidler and H. Eyring, "The Theory of Rate Processes," p. 480, (1941), McGraw-Hill, N. Y.

68. W. Kauzmann, Trans. AIME, (1941), 143, 57.

69. J. J. Gilman, J. Appl. Phys., (1973), 44, 675.

70. J. C. M. Li in "Frontiers in Materials Science" (L. E. Murr and C. Stein, eds.), p. 527, (1976), Marcel Dekker.

71. J. C. M. Li in "Metallic Glasses," A.S.M., p. 224, (1977), Cleveland, Ohio.

72. H. Eyring, J. Chem. Phys., (1936), 4, 283.

73. M. H. Cohen and D. Turnbull, J. Chem. Phys., (1959), 31, 1164; D. Turnbull and M. H. Cohen, J. Chem. Phys., (1961), 34, 120; and J. Chem. Phys., (1970), 52, 3038.

74. P. Ramachandrarao, B. Cantor and R. W. Cahn, J. Non-Cryst. Solids, (1977), 24, 109; and J. Mat. Sci., (1977), 12, 2488.

75. G. Adam and J. H. Gibbs, J. Chem. Phys., (1965), 43, 139.

76. H. S. Chen, J. Non-Cryst. Solids, (1976), 22, 135.

77. An approximate analysis has been made in ref. 51.

78. J. H. Dymond and B. J. Alder, J. Chem. Phys., (1966), 45, 2061.

79. A. S. Argon, "Plastic Deformation in Metallic Glasses," (1978), to be published in Acta Met.

Defense Documentation Center
Cameron Station
Alexandria, Virginia 22314 (12)

Office of Naval Research
Department of the Navy
Attn: Code 471 (3)
Code 105 (6)
Code 470

Director
Office of Naval Research
Branch Office
495 Summer Street
Boston, Massachusetts 02210

Director
Office of Naval Research
Branch Office
536 South Clark Street
Chicago, Illinois 60605

Office of Naval Research
San Francisco Area Office
760 Market Street, Room 447
San Francisco, California 94102

Naval Research Laboratory
Washington, D.C. 20390
Attn: Code 6000
Code 6100
Code 6300
Code 6400
Code 2627 (6)

Attn: Mr. F.S. Williams
Naval Air Development Center
Code 302
Warminster, Pennsylvania 18974

Naval Air Propulsion Test Center
Trenton, New Jersey 08628
Attn: Library

Naval Weapons Laboratory
Dahlgren, Virginia 22448
Attn: Research Division

Naval Construction Batallion
Civil Engineering Laboratory
Port Hueneme, California 93043
Attn: Materials Division

Naval Electronics Laboratory Center
San Diego, California 92152
Attn: Electronic Materials Sciences Div.

Naval Missile Center
Materials Consultant
Code 3312-1
Point Mugu, California 93041

Commanding Officer
Naval Ordnance Laboratory
White Oak
Silver Spring, Maryland 20910
Attn: Library

Naval Ship R. and D. Center
Materials Department
Annapolis, Maryland 21402

Naval Undersea Center
San Diego, California 92132
Attn: Library

Naval Underwater System Center
Newport, Rhode Island 02840
Attn: Library

Naval Weapons Center
China Lake, California 93555
Attn: Library

Naval Postgraduate School
Monterey, California 93940
Attn: Materials Sciences Dept.

Naval Air Systems Command
Washington, D.C. 20360
Attn: Code 52031
Code 52032
Code 320

Naval Sea System Command
Washington, D.C. 20362
Attn: Code 035

Naval Facilities
Engineering Command
Alexandria, Virginia 22331
Attn: Code 03

Scientific Advisor
Commandant of the Marine Corps
Washington, D.C. 20380
Attn: Code AX

Naval Ship Engineering Center
Department of the Navy
Washington, D.C. 20360
Attn: Director, Materials Sciences

Army Research Office
Box CM, Duke Station
Durham, North Carolina 27706
Attn: Metallurgy and Ceramics Div.

Army Materials and Mechanics
Research Center
Watertown, Massachusetts 02172
Attn: Res. Programs Office (AMXMR-P)

Commanding General
Department of the Army
Frankford Arsenal
Philadelphia, Pennsylvania 19137
Attn: ORDBA-1320

Office of Scientific Research
Department of the Air Force
Washington, D.C. 20333
Attn: Solid State Div. (SRPS)

Aerospace Research Labs
Wright-Patterson AFB
Building 450
Dayton, Ohio 45433

Air Force Materials Lab (LA)
Wright-Patterson AFB
Dayton, Ohio 45433

NASA Headquarters
Washington, D.C. 20546
Attn: Code RRM

NASA
Lewis Research Center
21000 Brookpark Road
Cleveland, Ohio 44135
Attn: Library

National Bureau of Standards
Washington, D.C. 20234

Attn: Metallurgy Division
Inorganic Materials Division

Atomic Energy Commission
Washington, D.C. 20545
Attn: Metals and Materials Branch

Defense Metals and Ceramics
Information Center
Battelle Memorial Institute
505 King Avenue
Columbus, Ohio 43201

Director
Ordnance Research Laboratory
P.O. Box 30
State College, Pennsylvania 16801

Director Applied Physics Lab.
University of Washington
1013 Northeast Fortieth Street
Seattle, Washington 98105

Metals and Ceramics Division
Oak Ridge National Laboratory
P.O. Box X
Oak Ridge, Tennessee 37830

Los Alamos Scientific Lab.
P.O. Box 1663
Los Alamos, New Mexico 87544
Attn: Report Librarian

Argonne National Laboratory
Metallurgy Division
P.O. Box 229
Lemont, Illinois 60439

Brookhaven National Laboratory
Technical Information Division
Upton, Long Island
New York 11973
Attn: Research Library

Library
Building 50, Room 134
Lawrence Radiation Laboratory
Berkeley, California

Professor G.S. Ansell
Rensselaer Polytechnic Institute
Dept. of Metallurgical Engineering
Troy, New York 12181

Professor H.K. Birnbaum
University of Illinois
Department of Metallurty
Urbana, Illinois 61801

Dr. E.M. Breinan
United Aircraft Corporation
United Aircraft Research Lab.
East Hartford, Connecticut 06108

Professor H.D. Brody
University of Pittsburgh
School of Engineering
Pittsburgh, Pennsylvania 15213

Professor J.B. Cohen
Northwestern University
Dept. of Material Sciences
Evanston, Illinois 60201

Professor M. Cohen
Massachusetts Institute of Technology
Department of Metallurgy
Cambridge, Massachusetts 02139

Professor B.C. Giessen
Northeastern University
Department of Chemistry
Boston, Massachusetts 02115

Dr. G.T. Hahn
Battelle Memorial Institute
Department of Metallurgy
516 King Avenue
Columbus, Ohio 43201

Professor R.W. Heckel
Carnegie-Mellon University
Scheney Part
Pittsburgh, Pennsylvania 15213

Dr. David G. Howden
Battelle Memorial Institute
Columbus Laboratories
505 King Avenue
Columbus, Ohio 43201

Professor C.E. Jackson
Ohio State University
Dept. of Welding Engineering
190 West 19th Avenue
Columbus, Ohio 43210

Professor G. Judd
Rensselaer Polytechnic Institute
Dept. of Materials Engineering
Troy, New York 12181

Dr. C.S. Kortovich
TRW, Inc.
23555 Euclid Avenue
Cleveland, Ohio 44117

Professor D.A. Koss
Michigan Technological University
College of Engineering
Houghton, Michigan 49931

Professor A. Lawley
Drexel University
Dept. of Metallurgical Engineering
Philadelphia, Pennsylvania 19104

Dr. H. Margolin
Polytechnic Institute of New York
333 Jay Street
Brooklyn, New York 11201

Professor K. Masabuchi
Massachusetts Institute of Technology
Department of Ocean Engineering
Cambridge, Massachusetts 02139

Dr. G.H. Meier
University of Pittsburgh
Dept. of Metallurgical and Materials
Engineering
Pittsburgh, Pennsylvania 15213

Professor J.W. Morris, Jr.
University of California
College of Engineering
Berkeley, California 94720

Professor K. Ono
University of California
Materials Department
Los Angeles, California 90024

Professor W.F. Savage
Rensselaer Polytechnic Institute
School of Engineering
Troy, New York 12181

Dr. C. Shaw
Rockwell International Corp.
P.O. Box 1085
1049 Camino Dos Rios
Thousand Oaks, California 91360

Professor O.D. Sherby
Stanford University
Materials Sciences Dept.
Stanford, California 94300

Professor J. Shyne
Stanford University
Materials Sciences Department
Stanford, California 94300

Dr. W.A. Spitzig
U.S. Steel Corporation
Research Laboratory
Monroeville, Pennsylvania 15146

Dr. E.A. Starke, Jr.
Georgia Institute of Technology
School of Chemical Engineering
Atlanta, Georgia 30332

Professor N.S. Stoloff
Rensselaer Polytechnic Institute
School of Engineering
Troy, New York 12181

Dr. E.R. Thompson
United Aircraft Research Lab.
400 Main Street
East Hartford, Connecticut 06108

Professor David Turnbull
Harvard University
Division of Engineering and Applied
Physics
Cambridge, Massachusetts 02139

Dr. F.W. Wang
Naval Ordnance Laboratory
Physics Laboratory
White Oak
Silver Spring, Maryland 20910

Dr. J.C. Williams
Rockwell International
Science Center
P.O. Box 1085
Thousand Oaks, California 91360

Professor H.G.F. Wilsdorf
University of Virginia
Department of Materials Science
Charlottesville, Virginia 22903

Dr. M.A. Wright
University of Tennessee
Space Institute
Dept. of Metallurgical Engineering
Tullahoma, Tennessee 37388